Progress in Neurobiology 221 (2023) 102398

Contents lists available at ScienceDirect

Progress in Neurobiology

journal homepage: www.elsevier.com/locate/pneurobio

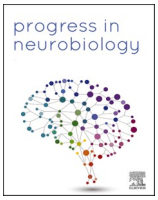

A large-scale brain network of species-specific dynamic human body perception☆

Baichen Li [a], Marta Poyo Solanas [a], Giuseppe Marrazzo [a], Rajani Raman [b,c], Nick Taubert [d], Martin Giese [d], Rufin Vogels [b,c], Beatrice de Gelder [a,e,*]

[a] Department of Cognitive Neuroscience, Faculty of Psychology and Neuroscience, Maastricht University, Maastricht 6200 MD, the Netherlands
[b] Laboratory for Neuro, and Psychophysiology, Department of Neurosciences, KU Leuven Medical School, Leuven 3000, Belgium
[c] Leuven Brain Institute, KU Leuven, Leuven 3000, Belgium
[d] Section for Computational Sensomotorics, Centre for Integrative Neuroscience & Hertie Institute for Clinical Brain Research, University Clinic Tübingen, Tübingen 72076, Germany
[e] Department of Computer Science, University College London, London WC1E 6BT, UK

ARTICLE INFO

Keywords:
FMRI
Body perception
Functional connectivity

ABSTRACT

This ultrahigh field 7 T fMRI study addressed the question of whether there exists a core network of brain areas at the service of different aspects of body perception. Participants viewed naturalistic videos of monkey and human faces, bodies, and objects along with mosaic-scrambled videos for control of low-level features. Independent component analysis (ICA) based network analysis was conducted to find body and species modulations at both the voxel and the network levels. Among the body areas, the highest species selectivity was found in the middle frontal gyrus and amygdala. Two large-scale networks were highly selective to bodies, dominated by the lateral occipital cortex and right superior temporal sulcus (STS) respectively. The right STS network showed high species selectivity, and its significant human body-induced node connectivity was focused around the extrastriate body area (EBA), STS, temporoparietal junction (TPJ), premotor cortex, and inferior frontal gyrus (IFG). The human body-specific network discovered here may serve as a brain-wide internal model of the human body serving as an entry point for a variety of processes relying on body descriptions as part of their more specific categorization, action, or expression recognition functions.

1. Introduction

Social species make extensive use of collaborative and competitive signals from conspecifics, allowing them to navigate successfully in the natural and social world. In the visual domain, social signals from faces and bodies are the central sources of information about conspecific presence, intentions, emotions, and actions. An extensive literature on face perception has already illustrated the importance of face perception for regulating interactions between nearby conspecifics (Panksepp, 1989). Like the face, the body is a rich and powerful means of social communication allowing quick and easy inferences about identity, gender, sex, physical health, attractiveness, emotional state, and social status. Body perception operates at a much longer distance than face perception and provides information about emotions, intentions, and actions relevant for social interaction (de Gelder et al., 2010). Yet, aside from studies of the body as a perceptual object category, our understanding of whole-body perception is still very limited (de Gelder and Poyo Solanas, 2021; Taubert et al., 2022). Despite a vast literature on the perception of action and intention that in fact assumes that body perception is involved (Orban et al., 2021), recent theories about social perception and social brain networks do not yet integrate findings from body perception studies (Patel et al., 2019; Pitcher and Ungerleider, 2021). Doing so may enrich and diversify those models.

In view of the relevance of bodily communication, one may expect that preferential processing routes exist in the brain for bodies (Downing and Kanwisher, 2001) and body expressions (de Gelder et al., 2010), just

☆ This work was supported by the European Research Council (ERC) FP7-IDEAS-ERC (Grant agreement number 295673; Emobodies), by the ERC Synergy grant (Grant agreement 856495; Relevance), by the Future and Emerging Technologies (FET) Proactive Program H2020-EU.1.2.2 (Grant agreement 824160; EnTimeMent) and by the Industrial Leadership Program H2020-EU.1.2.2 (Grant agreement 825079; MindSpaces).

* Correspondence to: Room 3.009, Oxfordlaan 55, 6229 EV Maastricht, the Netherlands.
E-mail address: b.degelder@maastrichtuniversity.nl (B. de Gelder).

https://doi.org/10.1016/j.pneurobio.2022.102398
Received 27 July 2022; Received in revised form 25 November 2022; Accepted 19 December 2022
Available online 21 December 2022

as has long been assumed for faces (Gross et al., 1969). Previous studies on body perception mainly addressed body category-specific processes in the ventral stream. In human studies, body selective areas were reported in the middle occipital/temporal gyrus termed the extrastriate body area (EBA) (Downing and Kanwisher, 2001), in the fusiform cortex termed the fusiform body area (FBA) (Peelen and Downing, 2005; Schwarzlose et al., 2005) and in the posterior superior temporal sulcus (pSTS) (Candidi et al., 2015). Body patches observed in monkeys with fMRI were mainly found along the STS (Vogels, 2022). Similar to the situation in human studies, there is a consensus that these different areas or patches presumably have different computational functions, but there is currently no accepted view on the specific role of each area or on its network organization in humans (de Gelder and Poyo Solanas, 2021) or in monkeys (Vogels, 2022).

Another central question concerns the contribution of body perception areas to the various perceptual functions that include body perception as well as action and expression perception. Studies focusing on body perception as part of research on action and emotion recognition revealed other areas in addition to those known from category-based studies. A comparison of expressive with neutral whole body still images (de Gelder et al., 2004, 2010) and studies using video images and controlling for action category (Grèzes et al., 2007) reported the posterior superior temporal sulcus (pSTS), temporoparietal junction (TPJ), frontal cortex and parietal motor regions (Pichon et al., 2009; Peelen et al., 2007; Grèzes et al., 2007), as well as the amygdala (AMG) (de Gelder and Poyo Solanas, 2021; Poyo Solanas et al., 2020b; Pichon et al., 2012). Notably, most of the clusters found in body expression studies were also reported in studies of the action observation network (Grèzes et al., 2007; Goldberg et al., 2014; Pichon et al., 2009), emotion (de Gelder et al., 2004; Borgomaneri et al., 2015) and included subcortical areas (Poyo Solanas et al., 2020b; Utter and Basso, 2008). The relation between category-selective areas and areas that seem to be involved in perceiving various functional roles of the body is still poorly understood.

To summarize, there are now some robust findings of body category selectivity in a few different brain areas in human and monkey. This raises the question of the underlying computational processes defining their respective roles, and of the interaction of the various body selective areas in hierarchical or parallel processing streams. For example, it is unclear what the computational processes presumably taking place in each body selective area are, and whether these are best understood at the level of each separate body selective area or, alternatively, at the level of interacting body areas and network functions.

Our goal was to discover the network organization of body perception in a data-driven way rather than by investigating local areas of category selectivity for bodies (Peelen and Downing, 2005) or for body expressions (de Gelder et al., 2010). We tested the hypothesis that there might be a basic body representation network that sustains different specific domains of human body perception. To investigate human body processing at the network organization level we used ultra-high field 7 T fMRI while participants viewed naturalistic dynamic videos of human and monkey faces, human and monkey bodies, and objects, as well as a scrambled version of each video as a control. Large-scale networks modulated by body processing were identified by the group independent component analysis (GICA), which has been widely used in resting-state and task-based fMRI studies (Du et al., 2017; Jarrahi et al., 2015; Jung et al., 2020). This GICA approach allowed us to separate single-voxel time courses into multiple components with maximized spatial independence. Here, the time course reflects a coherent fluctuation associated with an intrinsic network or associated with noise. Thus, by modeling the component time courses, we were able to reveal the networks modulated by our experimental conditions. Furthermore, to bring human body selectivity more narrowly in focus, we included monkey videos as the stimuli. Through the comparison with nonhuman species, it may offer insights into what exactly is coded in body selective areas and their network functions.

2. Results

Nineteen participants took part in the experiment. Two were excluded from further analysis due to large distortion of the functional or anatomical image. Twelve categories of videos (body/face/object * human/monkey * normal/scramble) were shown to the participants during the 7T fMRI scanning using a blocked design with six repetitions per category.

2.1. Univariate analysis

A random-effects general linear model (GLM) with all conditions as predictors was performed to find voxel-wise (human) body preference (see Methods). To control for low-level stimulus features such as the luminance, contrast, and the amount of local motion, we computed the contrast of [human body (normal - scramble)] > [human object (normal - scramble)]. The resulting statistical map was corrected using a cluster threshold statistical procedure based on Monte Carlo simulation (initial $p < 0.005$, alpha level = 0.05, iterations = 5000). Several body selective clusters were found in the extrastriate cortex (corresponded to EBA), fusiform cortex, pSTS, TPJ, and frontal gyrus, in agreement with previous body perception studies (de Gelder and Poyo Solanas, 2021; Ross et al., 2020) (Table 1, Fig. 1a). Subcortical regions including the amygdala, pulvinar, and caudate nucleus also showed body selectivity. The largest cluster corresponded to the right EBA (8355.84 mm^3) and the highest peak t-value was found in the right amygdala ($t(16) = 5.90$, $p < 0.001$). We further computed two additional low-level controlled contrasts to find a) human face selectivity by [human face (normal-scramble) > human object (normal-scramble)] and b) monkey body selectivity by [monkey body(normal-scramble) > monkey object (normal-scramble)]. After thresholding the statistical maps, overlaps were computed between the previously found human body clusters and the new contrasts. The largest overlaps were found in a) a left fusiform body cluster, where 100 % of voxels were also selective to the human face, and b) a right EBA cluster, where 39 % of voxels were also selective to the monkey body compared to objects (Table 1, S1 & S2).

To test the human body specificity of the body areas found above, we computed the low-level controlled contrast of [human body(normal-scramble) > monkey body (normal-scramble)] on each human body region of interest (ROI) defined above. Multiple body clusters were significantly species-selective, including EBA, fusiform, insula, middle frontal gyrus (MFG), precentral gyrus (corresponding to the dorsal premotor cortex, PMd), inferior parietal lobe (IPL) and amygdala (Fig. 1b). The cluster showing the highest human specificity was found in the MFG ($t(16) = 3.27$, $p = 0.005$, Table 1).

2.2. Independent component analysis

To study the network organization related to body perception, we applied a data-driven approach with group independent component analysis (GICA). Seventy-five independent components (ICs) were extracted from the preprocessed data (see Methods). A systematic pipeline was applied to exclude noise components and to find category-modulated networks. Five components were first removed due to an ICASSO *Iq* value lower than 0.8 (Himberg et al., 2004). The positive and negative parts of the remaining ICs were further divided into different IC sets, and the sign of the time courses and spatial maps of the negative ICs were flipped. Of the resulting 140 ICs, 16 positive ICs and 28 flipped ICs were identified as noise and were excluded due to white matter (WM) / cerebrospinal fluid (CSF) overlap larger than 10 %. Task relevance was modeled for each reconstructed IC time course using a GLM with the same design matrix as in the univariate analysis. Here, we assumed a positive hemodynamic response function (HRF) response for the cortical network time courses, thus the ICs / flipped ICs with a negative mean beta across all conditions were excluded from further analysis. Finally,

Table 1
Clusters found by random-effect group GLM. Contrast: human body (normal - scramble) > human object (normal - scramble).

ROI	Hemisphere	Peak Talairach coordinates:			Size (mm^3)	Peak t (df = 16)	Percentage of voxels significant for other contrasts		Averaged t-value for HB (N-S) > MB (N-S) (df = 16)
		x	y	z			HF (N-S) > HO (N-S)	MB (N-S) > MO (N-S)	
Precuneus	Right	6	-82	38	262	4.50			2.96 **
		5	-71	47	262	4.79			2.20 *
		3	-63	44	197	3.63			2.62 *
		6	-56	39	197	3.51			1.46
	Left	-6	-66	42	197	3.79			2.30 *
		-3	-62	49	786	3.77			1.83
		-15	-49	42	393	4.29			1.33
Intraparietal sulcus	Right	28	-64	36	426	4.85			2.33 *
Extrastriate cortex (EBA)	Right	37	-59	10	8356	4.98	4.31 %	38.82 %	1.91
		48	-52	9	262	3.52	25.00 %		1.35
		49	-46	0	4391	5.51	17.16 %	0.75 %	2.26 *
	Left	-50	-74	7	262	3.84			2.31 *
		-39	-63	11	459	4.11		14.29 %	1.95
		-60	-59	6	393	3.78	33.33 %		2.18 *
		-59	-56	-3	524	4.20			2.57 *
		-47	-54	8	1180	4.02			1.41
Fusiform (FBA)	Right	38	-50	-21	229	4.31	14.29 %		2.33 *
		34	-42	-18	360	4.94			2.30 *
		36	-27	-17	623	4.15			2.11
	Left	-37	-41	-20	229	3.62	100.00 %		2.25 *
Posterior superior temporal sulcus	Right	45	-49	11	262	4.09			1.53
		50	-34	10	295	4.08	88.89 %		1.83
Temporoparietal junction	Right	48	-47	15	393	3.85			2.47 *
		52	-36	19	1114	4.47	14.71 %	2.94 %	1.62
Superior parietal lobule	Left	-3	-46	65	295	5.64			0.78
Inferior parietal lobule	Left	-54	-41	46	1409	4.81			2.56 *
Pulvinar	Right	10	-31	2	492	5.35	26.67 %		1.13
Central Sulcus	Left	-37	-20	49	197	3.97			1.46
Precentral gyrus (M1)		48	-10	53	688	5.04			0.90
Caudate	Right	18	-10	25	262	4.12			1.22
Inferior precentral sulcus (PMd)	Right	40	-9	38	360	4.20	27.27 %		1.88
		32	-7	53	1016	5.07			2.43 *
Amygdala	Right	22	-4	-10	819	4.64	80.00 %		1.63
		18	-2	-10	328	5.90			2.77 *
	Left	-20	-6	-10	1049	4.86	40.63 %		1.96
Superior frontal gyrus (SMA/ pre-SMA)	Right	5	1	64	197	3.74			2.41 *
		10	2	58	229	4.66			1.46
	Left	-9	-10	58	360	5.09	72.73 %		1.48
Anterior superior temporal gyrus	Left	-30	6	-22	295	4.08	33.33 %		1.50
Insula	Left	-34	12	0	426	4.98			2.31 *
Middle frontal gyrus	Left	-31	34	25	393	3.93			1.84
		-39	40	26	262	4.48			3.27 **
		-35	41	34	295	4.10			2.62 *
		-30	55	22	197	3.91			2.33 *

Statistic maps were corrected using a cluster-threshold statistical procedure based on Monte-Carlo simulation (initial $p < 0.005$, alpha level = 0.05). Abbreviations in the contrasts: H: human; M: monkey; B: body; O: object; N: normal; S: scramble. * : $p < 0.05$, **: $p < 0.01$, *** : $p < 0.001$

19 positive ICs and 31 flipped ICs were used in further analyses.

To investigate condition-specific modulations within these ICs, several contrast analyses were conducted with the estimated betas from the IC time courses. For the first contrast of [normal human body > normal human object], we found only one network showing significant selectivity for human bodies after multiple comparison corrections (IC42, Fig. 2a, $t(16) = 3.97$, Benjamini-Hochberg False Discovery Rate corrected $q < 0.05$, right-tailed). The network (referred to as the rSTS network for abbreviation) covered right-lateralized regions including EBA, fusiform, STS, TPJ, IPL, MFG, precentral gyrus (PrCG), inferior frontal gyrus (IFG) and pulvinar, as well as bilateral clusters around amygdala, insula and supramarginal gyrus (SMG). Further inspection of the estimated betas revealed a significant preference of this network for human faces over monkey faces ($t(16) = 2.40$, $p = 0.029$, two-tailed) and for human bodies over monkey bodies ($t(16) = 2.92$, $p = 0.010$, two-tailed) (Fig. 2c). Further inspection of the beta plot revealed a structural response profile where the highest response was found for the human face, then the human body and the monkey face, and the monkey body came to the last (Fig. 2c). However, the response difference was not significant between human body and human face conditions ($t(16) = 1.77$, $p = 0.096$, two-tailed).

For the second contrast analysis, we controlled for low level features. Using the contrast of [human body (normal - scramble) - human object (normal - scramble)]), in addition to the rSTS network ($t(16) = 2.93$, corrected $q < 0.05$, right tailed), another IC also showed human body selectivity (IC04, Fig. 2b, $t(16) = 3.29$, corrected $q < 0.05$, right-tailed). The spatial map of this component revealed a lateral occipital cortex dominant network (referred to as the LOC network for abbreviation), which also included bilateral fusiform, superior parietal lobe (SPL), pSTS/TPJ, pulvinar and amygdala. However, no human specificity was found either by the contrast of [human body (normal - scramble)] > [monkey body (normal - scramble)] ($t(16) = 1.98$, $p = 0.065$, two-

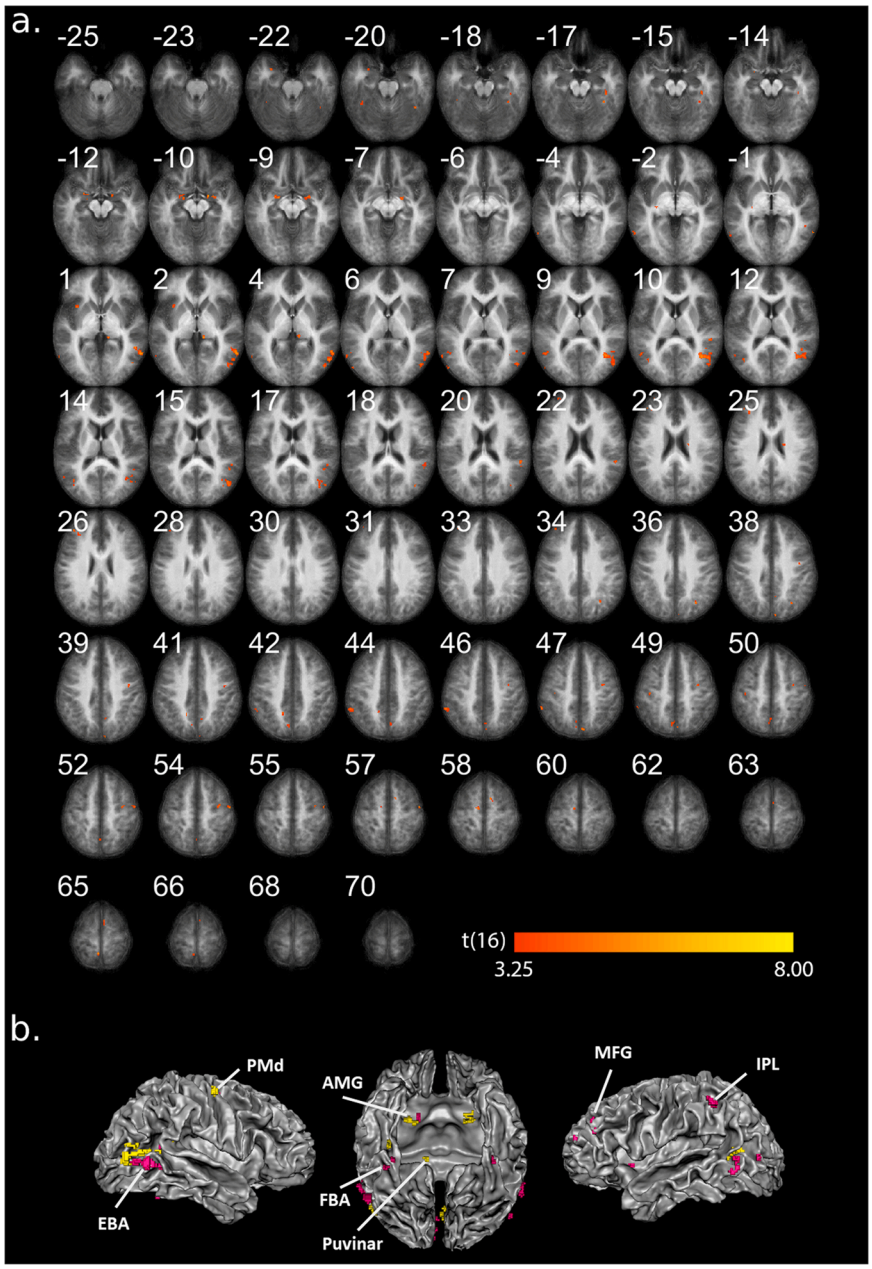

Fig. 1. Group univariate results. **(a)** Contrast of [HB(N-S) > HO(N-S)] (only positive values are shown). The resulting statistical map was corrected using a cluster-threshold statistical procedure based on Monte-Carlo simulation (initial $p < 0.005$, alpha level = 0.05). The number on each slice indicates the z-coordinate of Talairach space. **(b)**. The same clusters in (a) projected to the cortical mesh. ROI-level significant for contrast [HB(N-S) > MB (N-S)] are colored in pink (uncorrected $p < 0.05$, Table 2). Abbreviations in the contrasts: H: human; M: monkey; B: body; O: object; N: normal; S: scramble.

tailed), or by the contrast of [human face (normal - scramble)] > [monkey face (normal - scramble)] ($t(16) = 0.51$, $p = 0.615$, two-tailed) (Fig. 2d). The contrast of [human body (normal - scramble)] > [human face (normal - scramble)] revealed a significant preference for human body over human face ($t(16) = 4.12$, $p < 0.001$, two-tailed). Overlap between the rSTS network and the LOC network was found around the temporo-occipital region, covering the clusters of EBA, fusiform, pSTS, TPJ as well as pulvinar and amygdala (Fig. 2e), which were also found by univariate analyses.

To further investigate condition-specific modulations on the node connectivity of the above-mentioned networks, we repeated the same ICA procedure after regressing out the activity of one category from the time courses and we compared the condition-omitted spatial maps and the original one for the same network. With this comparison, the condition dependence of the nodes can be then identified as decreased network weights after the omission. As a result, significant drops in IC weight were detected in EBA, pSTS/TPJ, PrCG (corresponding to PMd/PMv) and IFG in the rSTS network after the normal human body blocks were omitted (Table 2, Fig. 3). Both the largest cluster and the peak t-value were found in IFG (largest V = 14647.30 mm^3; highest peak $t(16) = 7.60$, $p < 0.001$). For the LOC network, the connectivity weight drops were observed mainly around bilateral EBA (Table 2, Fig. 3), with the largest cluster and peak t-value found in right EBA (largest V = 6815.74 mm^3; highest peak $t(16) = 6.70$, $p < 0.001$).

In addition to defining the body nodes, we reconstructed the networks separately after regressing out the human face condition and the monkey body condition. Within the defined body nodes, we first searched for the voxels showing significant connectivity decrease for human-face-regressed and monkey-body-regressed maps. For the rSTS network (Fig. 4a), the human face dependence was found in the right pSTS, TPJ, PMd and IFG body nodes (uncorrected $p < 0.05$, Fig. 4b). Monkey body dependence was only found around the right EBA and pSTS body node (uncorrected $p < 0.05$, Fig. 4c). Next, to find voxels with unique dependence on the human body, we conducted a conjunction analysis with the contrast of [decrease(human body) > decrease (human face)] and [decrease (human body) > decrease (monkey body)]

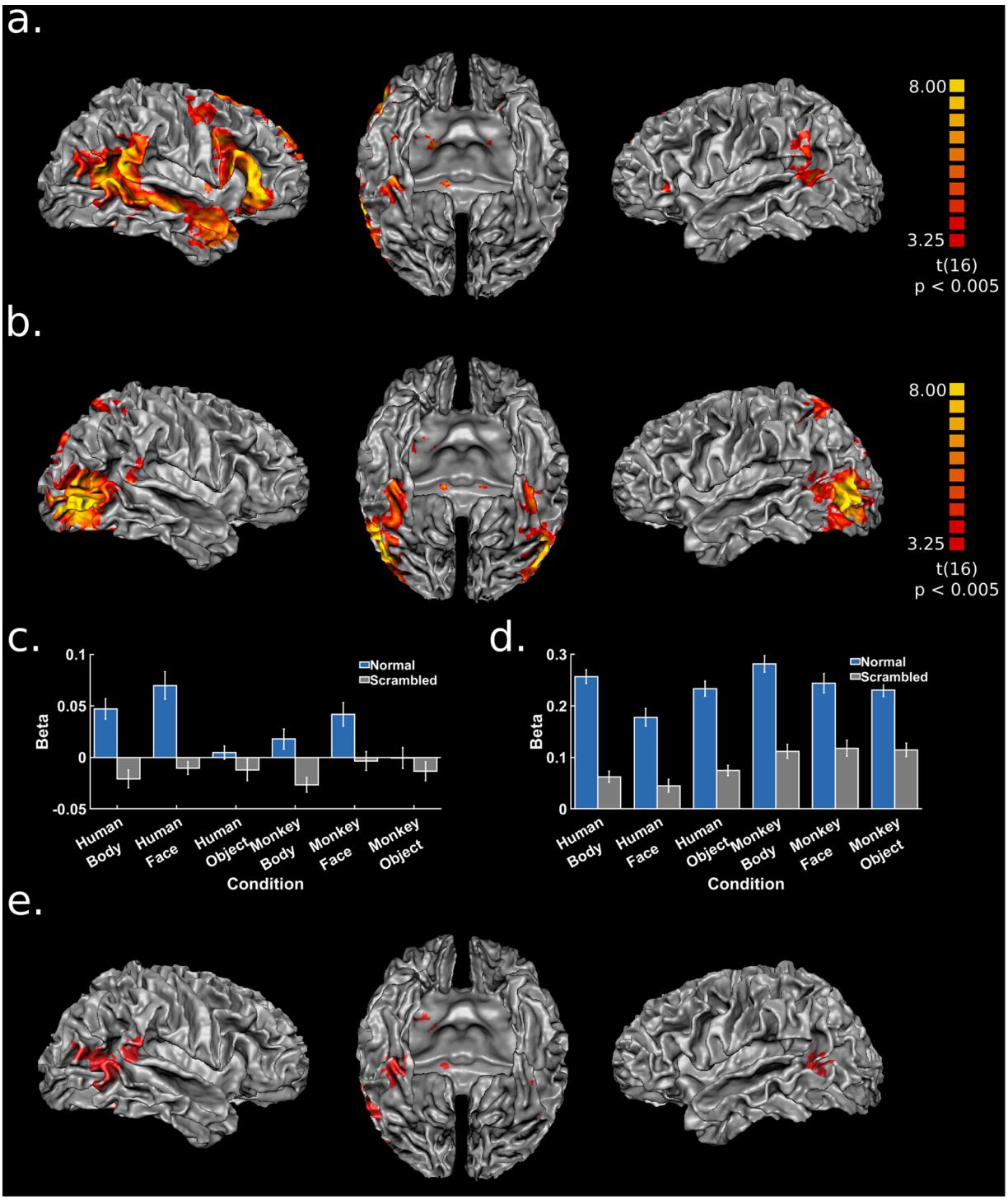

Fig. 2. Networks extracted by group-ICA. The individual IC maps were z-transformed and averaged across all runs for each participant. A group t-test against zero was computed using the z-scored maps of each subject. The resulting statistical map was corrected using a cluster-threshold statistical procedure based on Monte-Carlo simulation (initial $p < 0.005$, alpha level = 0.05). **(a)** & **(c)**. rSTS network and its beta plot. **(b)** & **(d)**. LOC network and its beta plot. **(e)**. The overlap between the two networks.

within the body nodes. As a result, significant voxels were found in the bilateral EBA, right TPJ, PMv, SMA, SFG, and IFG body nodes (uncorrected $p < 0.05$, Fig. 4d). For the LOC network, voxels with monkey-body or human-face-dependent voxels were found in bilateral EBA nodes, while the human-body-specific voxels were mainly found in the left EBA node.

3. Discussion

Using dynamic multispecies stimuli, 7 T fMRI scanning and data-driven methods we investigated body selective areas and their species specificity and category selectivity and focused on the network organization of body perception. We discovered two large-scale networks specifically modulated by human body videos, the LOC network and the rSTS network. We briefly discuss these new findings on body selectivity

Table 2
Clusters found by original ICA - HB-omitted ICA.

ROI	Hemisphere	Peak Talairach coordinates:			Size (mm^3)	Peak t (df = 16)
		x	y	z		
rSTS network						
Extrastriate cortex (EBA)	Right	58	-54	-4	492	4.60
		56	-52	2	2736	5.32
	Left	-43	-55	11	360	4.73
Posterior superior temporal sulcus	Right	53	-51	13	967	5.10
		54	-39	2	852	5.04
Temporoparietal junction	Right	53	-49	25	229	4.14
		60	-44	14	557	4.43
		58	-38	29	590	5.33
		57	-38	22	1802	4.66
Middle superior temporal sulcus	Right	42	-28	-1	328	5.17
Anterior superior temporal sulcus	Right	50	-6	-16	197	4.27
Inferior precentral sulcus (PMd/PMv)	Right	46	-2	52	229	3.56
		42	2	46	1311	5.12
		35	6	29	229	4.35
Superior frontal gyrus (SMA/pre-SMA1)	Right	7	5	58	1016	5.62
Inferior frontal gyrus	Right	53	27	18	14,647	7.60
Superior frontal gyrus	Right	10	28	51	393	4.09
		14	49	27	721	4.87
LOC network						
Extrastriate cortex (EBA)	Right	47	-70	2	6816	6.70
		56	-50	4	197	4.74
	Left	-49	-71	2	2621	6.12
		-43	-63	10	557	3.95
		-52	-55	7	262	3.94

Statistic maps were corrected using a cluster-threshold statistical procedure based on Monte-Carlo simulation (initial $p < 0.005$, alpha level = 0.05). Abbreviations in the contrasts: H: human; M: monkey; B: body; O: object; N: normal; S: scramble. * : $p < 0.05$, * *: $p < 0.01$, * ** : $p < 0.001$

and species specificity in the light of the literature and then address the main findings. Finally, we propose an interpretation of the possible functions of the two body perception networks.

3.1. Multiple areas of body selectivity

Our univariate results provide the first complete picture based on ultra-high field scanning of human body-specific dynamic body perception. Concerning the best know body selective areas EBA and FBA, the novel result here is that a subset of clusters is species-specific for human bodies. A possible basis for human body specific coding may be that these areas compute features that are more characteristic of human body movements, for example, because they abide by biomechanical constraints of human body posture and motion. A related basis for human-specificity also at the feature level may be that the coding in these two areas is partly driven by expression perception. For example, the features that deliver some affective information embedded in human body expressions (Poyo Solanas et al., 2020a; b) may be absent in monkey bodies.

For two other areas, pSTS and TPJ, we also found subclusters that are human-body-specific. This may provide a conceptual basis for previous findings on the biological motion of faces and bodies (Patel et al., 2019; Polosecki et al., 2013; Yovel and O'Toole, 2016). There is recent evidence that these two regions may be involved in the predictive coding of biomechanical movements (Geng and Vossel, 2013; Koster-Hale and Saxe, 2013). pSTS/TPJ is involved in the generation of model-based predictions of biomechanical trajectories of moving faces or body parts (Patel et al., 2019; Geng and Vossel, 2013; Koster-Hale and Saxe, 2013). Other clusters were found in frontoparietal areas including SPL, intraparietal sulcus (IPS), as well as PMd and belonging to the dorsal frontoparietal network (dFPN). Those regions may be involved in the dynamic representation of the kinematic properties of movement plans (Ptak et al., 2017).

Finally, subcortical clusters were found in the pulvinar and amygdala. The amygdala plays a role in affective stimulus perception also when the images are whole body expressions (Hadjikhani and De Gelder, 2003). However, its exact role is still a matter of debate as it may depend on factors like stimulus visibility (Pessoa et al., 2006), task (Pichon et al., 2012), and the intactness of amygdala (Hortensius et al., 2017). Similarly, Padmala et al. (2010) showed a correlation between pulvinar responses and stimulus detection, especially for affective conditions. It remains a matter of debate whether the amygdala activates relatively autonomously as assumed by the notion of a pathway involving superior colliculus and pulvinar to amygdala, or whether the critical role of amygdala and pulvinar is to coordinate activity in cortical networks (Pessoa and Adolphs, 2010).

3.2. Network-based body selectivity

Our ICA analysis discovered two networks with significant selectivity for bodies and very different response profiles for other categories. The connectivity of these networks is significantly influenced by bodies and shows human body specificity, especially the rSTS network.

3.2.1. LOC network

The LOC network mainly consisted of a large cluster in the lateral occipital cortex and the fusiform cortex, covering most of the previously defined category-selective areas (Grill-Spector and Sayres, 2008). The classical view of category-selective areas is that these areas compute the entry-level representation of the preferred category and that these category computations are not dependent on low level features. But the current understanding of the relationship between low-level features (contrast edges, local motion, luminance, differences in spatial frequency) and high-level category-defining representation is limited (Long et al., 2018; de Gelder and Poyo Solanas, 2021). In this respect, it is interesting to see that the body selectivity of this network emerged when taking the respective scrambled control conditions into account. Thus, the LOC network may be selective for specific properties of the body videos (Grill-Spector and Weiner, 2014) and this selectivity may be partly based on midlevel features like human body specific movement or postural characteristics over time (Poyo Solanas et al., 2020a; b).

3.2.2. rSTS network

The rSTS network showed a right hemisphere-dominant coverage including EBA, FBA, STS, PMd/PMv and IFG. Its other nodes such as the premotor cortex, medial prefrontal cortex, TPJ, and amygdala, have also been related to social cognition (Saxe and Kanwisher, 2003; Schurz et al., 2014; Van Overwalle, 2009; Young et al., 2010; Patel et al., 2019; Alcalá-López et al., 2018). Most notably, this network showed the highest response for human faces and human bodies, followed by monkey faces, and lastly monkey bodies (Fig. 2c). While the contrast was not significant between human bodies and faces, significantly higher responses were found for human videos than for the monkey ones. Thus, the rSTS network may involve the processing of human-specific social information.

3.2.3. Node-level body modulation within networks

We were also interested in identifying the nodes within each network that were involved in body processing compared to the other stimulus conditions. Using condition-omitted ICA, we first found body modulations of node connectivity only in the bilateral posterior EBA in the LOC network. Similarly, EBA nodes were also body-modulated in the rSTS network, which overlapped with the anterior EBA cluster found to be human-specific in our univariate analysis. It should be noted that while

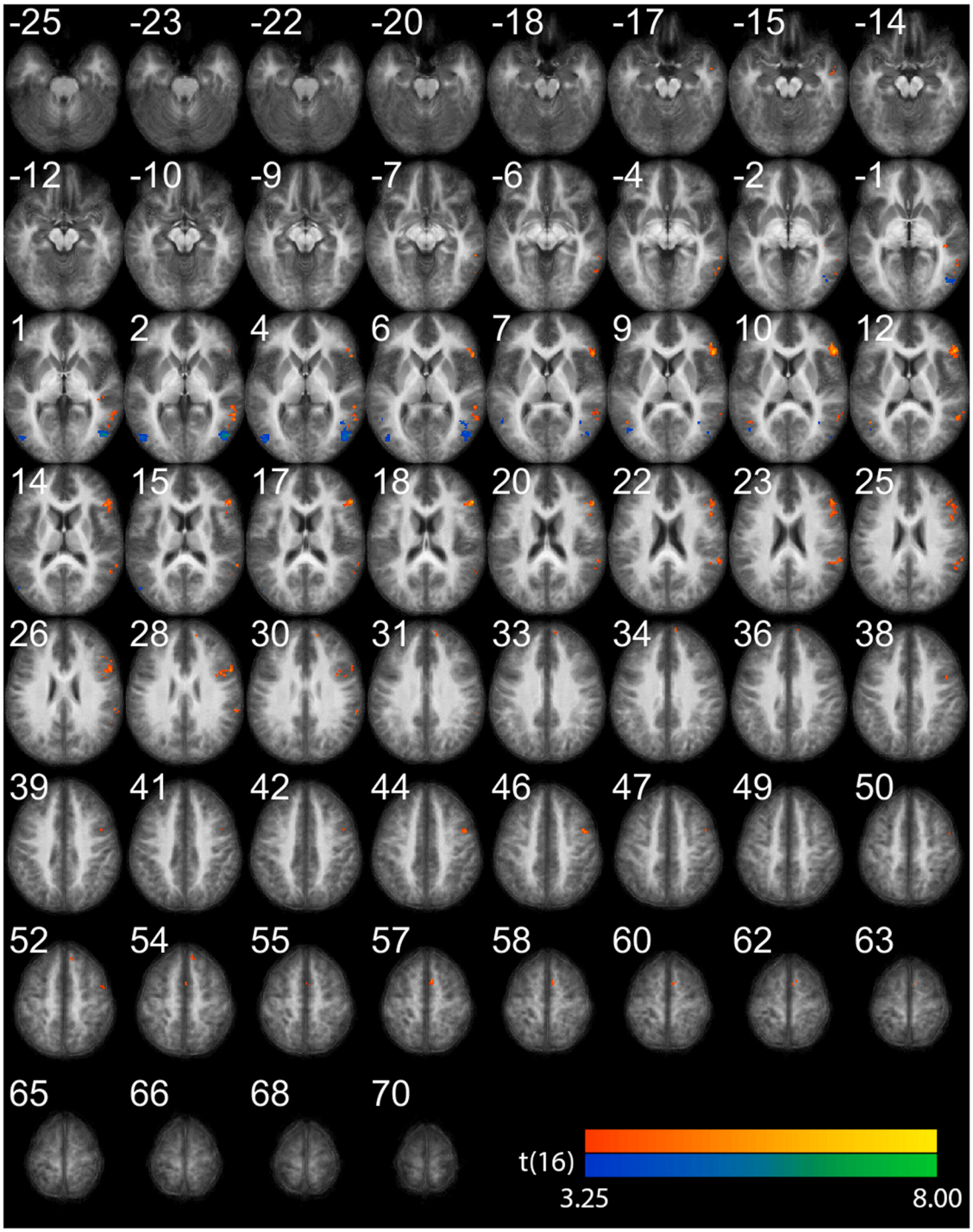

Fig. 3. Connectivity drops calculated by original ICA – HB-omitted ICA for the two networks. The group statistical map was corrected using a cluster-threshold statistical procedure based on Monte-Carlo simulation (initial $p < 0.005$, alpha level = 0.05) and masked by thresholded networks in Fig. 2a&b separately. Red clusters indicate significant connectivity drops for rSTS network, and blue clusters indicate drops in LOC network.

the anterior EBA was covered by both the LOC and rSTS networks, the posterior EBA was only covered by the LOC network. This suggests that the posterior and anterior EBA may be involved in different types of information flow during body processing, possibly reflecting different computations of the EBA subparts in each network since EBA is a complex area covering three heterogeneous regions surrounding the human motion-selective complex (hMT+) (Weiner and Grill-Spector, 2011).

In the rSTS network, more body related involvement was found beyond EBA, including TPJ, premotor cortex, frontal gyrus, and the clusters along STS. A notable property of the current rSTS network is its right lateralization, which was previously only found in studies on face processing (De Winter et al., 2015; Sato et al., 2019; Yokoyama et al., 2021). Interestingly, other studies suggested an opposite view of the lateralized social network, with the left hemisphere related to the detailed evaluation of social signals and the right hemisphere to rapid automatic detection of the high valence stimuli (Alcalá-López et al., 2018). Such contrasting views may indicate that, between the low-level visual features and the extraction of semantic information, there are intermediate stages during the processing, especially of the affective social signal.

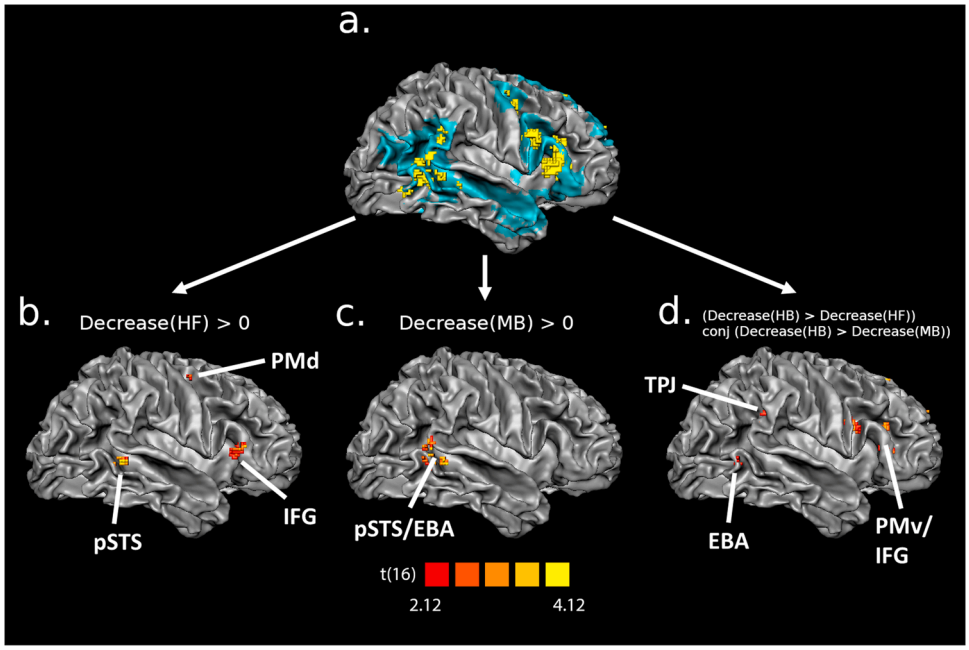

Fig. 4. Dependence properties revealed by the weight decreases for the rSTS body nodes. **(a)**. The rSTS nodes in Fig. 3 projected to cortical mesh with blue shadows indicating the network coverage. **(b)**. Node voxels showing human face dependence. **(c)**. Node voxels showing monkey body dependence. **(d)**. Node voxels showing human-specific body dependence. Abbreviations in the contrasts: H: human; M: monkey; B: body; F: Face.

3.2.4. The subnetwork for human-specific body processing

To consolidate the evidence of human body specificity of the nodes detected above, we further searched for the voxels with distinct or shared dependence for human bodies compared to the human face and monkey body. The result showed that among the rSTS body nodes, voxels within the EBA, TPJ, PMv, SMA, SFG and IFG nodes showed significantly larger connectivity decreases for the human-body-regressed network than for the human-face- or monkey-body-regressed ones. This result suggested a subnetwork for human-specific body processing.

While most of the nodes found in the subnetwork have been commonly described as "multifunctional regions" (Grabenhorst and Rolls, 2011; Nachev et al., 2008; Saxe and Kanwisher, 2003), the connectivity changes among these regions may suggest a specific function. The most intriguing part of this subnetwork may be the TPJ and IFG pair. Connected by the third tract of the superior longitudinal fasciculus (SLF III), TPJ and IFG have been traditionally linked to the ventral attention network and specifically to attentional processes related to stimulus orientation (Vossel et al., 2014; Corbetta et al., 2008). However, recent studies have suggested a more complicated role of TPJ and IFG in social cognition (Patel et al., 2019, 2021; Hartwigsen et al., 2019) as also suggested by the fact that lesions in SLF III may result in embodiment dysfunctions (Errante et al., 2022). Here, while we found multiple body nodes around IFG and TPJ (Fig. 4a), only a subset of the nodes showed human-body specificity. This result is in line with the anatomical and functional diversity within the two regions (Cheng et al., 2021; Igelström and Graziano, 2017; Patel et al., 2019; Hartwigsen et al., 2019; Briggs et al., 2019). In detail, body nodes were found in both the pars opercularis (OP) and the pars triangularis (TRI) of IFG (Fig. 4a), and while some of the TRI clusters were also modulated by faces (Fig. 4b), the OP cluster was exclusively involved for human body (Fig. 4d). Similarly, body-specific modulations were only found in the anterior part of TPJ (TPJa), as defined by Mars et al. (2011). However, when moving to the boundary of TPJa, another TPJ body node started to show monkey body modulations (Fig. 4c). Previous studies have suggested the involvement of both TPJa and OP in spatial attention or model-based prediction processes (Patel et al., 2019; Hartwigsen et al., 2019). A recent study also found that the lower TPJa was also modulated by the prediction errors when viewing moving objects (Scheliga et al., 2022). Thus, the concurrence of the TPJa node and the OP node may involve some human-specific movement processing, such as the encoding or predicting the trajectories of moving body parts.

3.2.5. Correspondence and intersection between the two networks

An interesting question concerns the communication between the two networks. Thus, we further inspected the overlaps between the LOC and rSTS networks, aiming to find a potential bridge linking the lower- and higher-level processing of body stimuli. Besides the regions of the EBA and FBA, the most notable cortical intersections of the two networks were found around pSTS/TPJ, which is again compatible with the notion of pSTS/TPJ as a middle-station between networks mentioned above. The connection between lower- and higher-level information can also be found in the pulvinar region, which was found as a main subcortical intersection between our two networks. As pointed out by recent studies, the ventral part of the pulvinar is sensitive to low-level temporal structures, while the dorsal part is selective to more integrated information (Arcaro et al., 2018; Hasson et al., 2008, 2015). Consistent with this, only the ventral pulvinar was involved in the LOC network, while both the ventral and dorsal parts were found in the rSTS network. In conclusion, pSTS/TPJ and pulvinar may play an important role during information exchanges between the lower-level feature system and the higher-level social information system.

3.3. Relation between category, action and emotion perception and the social brain networks

In contrast with existing proposals the present rSTS network was found using a data-driven approach. Previous studies have proposed somewhat similar networks based on meta-analyses or used data from the human connectome project (e.g., Alcalá-López et al., 2018). One is the action observation network (AON, Caspers et al., 2010), with similar nodes around EBA, IFG, and PM. However, compared to the AON, our rSTS network showed a highly right-lateralized distribution that covered a large area in the right STS, which is missing in the AON. Another recent proposal on the third visual pathway stressed the role of STS in processing social information. However, this misses the links between the

STS route and the other cortical regions (Haak and Beckmann, 2018). Still, another network proposal that has the best compatibility with our network results is a TPJ/pSTS-centered social cognition network (Patel et al., 2019). In this network, the TPJ/pSTS served as a hub receiving the input from the lower visual regions while sending integrated information to a social cognition network. Moreover, the study suggested that the third pathway of STS may serve as an input to the hub of TPJ/pSTS, thus also explaining the involvement of the large STS in our network. These findings are in line with the view that the pSTS/TPJ may serve as a hub node for integrating different functional networks (Patel et al., 2019). Our results now add that this hub function may to an important extent be based on receiving inputs from EBA/FBA.

4. Materials and methods

4.1. Participants

Nineteen healthy participants (mean age = 24.58; age range = 19–30; 6 males, all right handed) took part in the experiment. All participants had a normal or corrected-to-normal vision and no medical history of any psychiatric or neurological disorders. All participants provided informed written consent before the start of the experiment and received a monetary reward (vouchers) or course credits for their participation. The experiment was approved by the Ethical Committee at Maastricht University and was performed in accordance with the Declaration of Helsinki.

4.2. Stimuli

The materials used in this experiment consisted of 1-second-long grayscale videos of bodies, faces, and objects edited from original human and monkey recordings. The body and face videos depicted either a human or a monkey performing naturalistic full-body or facial movements. Object stimuli consisted of two sets of moving artificial objects with the aspect ratio matched to either human bodies or monkey bodies. The size of the stimuli was 3.5 * 3.5 degrees of visual angle for human faces, 3.5 * 7.5 degrees for human bodies and objects, and 6 * 6 degrees for monkey faces, bodies and objects. The human videos were selected from the set originally developed in Kret et al. (2011), in which all actors were dressed in black and performed natural full body / face expressions against a greenscreen background. The expressions contained anger, fear, happiness, as well as neutral expressions such as pulling nose or coughing. The monkey videos were taken from footage of rhesus monkeys from the KU Leuven monkey colony and also from a published comparative study of facial expressions (Zhu et al., 2013). The body videos included grasping, picking, turning, walking, threatening, throwing, wiping, and initiating jumping, while the face videos included chewing, lip-smacking, fear grin, and threat. For human and monkey videos, a variety of both emotional and neutral poses were included, and the face information within each body video was removed by applying Gaussian blurring.

After removing the original background, the videos were cut to 1 s duration (60 frames/s) and overlaid on a full-screen dynamic white noise background spanning 17.23 * 10.38 degrees of visual angle. The background consisted of small squares of 3 by 3 pixels of which the gray level was randomly sampled from a uniform distribution at a rate of 30 Hertz. To directly control for low-level feature differences among the three categories (bodies, faces and objects), we included mosaic-scrambled videos as an additional set of stimulus conditions. The mosaic scrambled stimuli destroyed the whole shape and global motion of the dynamic bodies, faces, and objects, but had identical local motion (within 14 pixels wide squares), luminance, contrast, and non-background area as the original movies. This resulted in a total of twelve experimental conditions (human/monkey * body/face/object * normal/scrambled). There were ten different stimuli per condition, which resulted in 120 unique videos.

4.3. Experimental design

During the experiment, stimuli were presented following a block-design paradigm. For each block, ten videos of the same experimental condition were presented once for 1000 ms in random order with an inter-stimulus-interval (ITI) of 500-ms consisting of a uniform gray canvas. Two blocks per condition were randomly presented within each run. Between blocks, there was a jittered interval of 11 s where a blank canvas was presented. For each participant, we collected three experimental runs, resulting in six repetitions per condition. At the beginning and the end of each run, a white noise block was presented with only the dynamic noise background but no actual stimulus (ten videos of 1-second with an ITI of 500-ms). Ultimately, for each run we collected 735 functional volumes resulting in approximately 12 min of scanning time.

During the experiment, participants were instructed to keep fixation on a cross presented at the center of the screen throughout the whole run. Participants' attention was controlled by adding two catch blocks in each run, in which the fixation cross changed its shape to a circle during a random trial. The participants were asked to press a button with the right index finger when detecting the fixation shape change. The category of each catch block was randomly chosen from the twelve experimental conditions, and all of the catch blocks were removed from further data analysis to rule out response-related confounds.

The experiment was programmed using the Psychtoolbox (https://www.psychtoolbox.net) implemented in Matlab 2018b (https://www.mathworks.com). Stimuli were projected onto a screen at the end of the scanner bore with a Panasonic PT-EZ57OEL projector (screen size = 30 * 18 cm, resolution = 1920 * 1200 pixel). Participants viewed the stimuli through a mirror attached to the head coil (screen-to-eye distance = 99 cm, visual angle = 17.23 * 10.38 degrees). The whole experiment lasted for 40 min. The same participants underwent another round of scanning for a different experiment which is not reported here.

4.4. fMRI data acquisition

All images were acquired with a 7 T MAGNETOM scanner at the Maastricht Brain Imaging Centre (MBIC) of Maastricht University, the Netherlands. Functional images were collected using the T2 * -weighted multi-band accelerated EPI 2D BOLD sequence (TR/TE = 1000/20 ms, multiband acceleration factor = 3, in-plane isotropic resolution = 1.6 mm, number of slices per volume = 68, matrix size = 1152 * 1152, volume number = 735). T1-weighted anatomical images were obtained using the 3D-MP2RAGE sequence (TR/TE = 5000/2.47 ms, Inverse time TI1/I2 = 900/2750 ms, flip angle FA1/FA2 = 5/3°, in-plane isotropic resolution = 0.7 mm, matrix size = 320 * 320, slice number = 240). Physiological parameters were recorded via pulse oximetry on the index finger of the left hand and with a respiratory belt.

4.5. fMRI image preprocessing

Anatomical and functional images were preprocessed using the Brainvoyager 22 (Goebel, 2012) and the Neuroelf toolbox in Matlab (https://neuroelf.net/). For anatomical images, brain extraction was conducted with INV2 images to correct for MP2RAGE background noise. The resolution was then downsampled to 0.8 mm for better alignment to the 1.6 mm resolution of functional images. For functional images, the preprocessing steps included EPI distortion correction (Breman et al., 2020), slice scan time correction, 3D head-motion correction, and high-pass temporal filtering (GLM with Fourier basis set of 3 cycles, including linear trend). Coregistration was first conducted between the anatomical image and its most adjacent functional run using a boundary-based registration (BBR) algorithm (Greve and Fischl, 2009), and all the other functional runs were coregistered to the aligned run. Individual images were normalized to Talairach space (Collins et al., 1994) with 3 mm Gaussian spatial smoothing. Trilinear/sinc interpolation was used in the motion correction step, and sinc interpolation was

used in all of the other steps.

Physiological parameters were collected as the confounds of functional imaging data. The physiological data were preprocessed using the RETROspective Image CORrection (RETROICOR; Glover et al., 2000; Harvey et al., 2008) pipeline, which uses Fourier expansions of different orders for the phase of cardiac pulsation (3rd order), respiration (4th order) and cardio-respiratory interaction (1st order). 18 physiological confounds were finally created for each participant.

For visualization, we created a cortical mesh from a single subject in Talairach space. The subject anatomical image first underwent a fine-tuned deep-learning-based segmentation implanted in Brainvoyager. The resulting gray/white matter labeling image was then aligned to the group-averaged anatomical image with SyN algorism using the toolbox of Advanced Normalization Tools (ANTs; Avants et al., 2022). The group cortical mesh was finally created from the aligned labeling image.

The anatomical labeling of the following was according to the Talairach Daemon (http://www.talairach.org/daemon.html) in combination with the Multilevel Human Brain Atlas (https://ebrains.eu/service/human-brain-atlas). Since in our study the anatomical resolution was 0.8 mm instead of 1 mm as used in Talairach Daemon, we also searched for the nearest gray matter in the labeling to account for the interpolation of the Talairach coordinates.

4.6. Univariate analysis

A random-effects general linear model was performed to find the voxel-wise categorical preference. In the design matrix, each condition predictor was modeled as a boxcar function with the same duration of the block and convolved with the canonical hemodynamic response function (HRF). Physiological and motion confounds were added as nuisance repressors.

Body selective areas were defined by the contrast analysis of [human body (normal - scrambled) > human object (normal - scrambled)]. The term of (normal - scramble) aimed to rule out influences from low-level stimulus features. The resulting statistical map was corrected using a cluster-threshold statistical procedure based on the Monte-Carlo simulation (initial $p < 0.005$, alpha level = 0.05, iteration = 5000).

Besides the body contrasts, we calculated two additional low-level controlled contrasts for human face selectivity [human face (normal - scrambled) > human object (normal - scrambled)] and cross-species body selectivity [monkey body (normal - scrambled) > monkey object (normal - scrambled)]. The statistical maps were thresholded in the same manner as for the body contrasts, and the overlaps were computed for each previous body cluster and the new contrast, resulting in a proportion of voxels showing other selectivity in each body cluster.

To test the species-selectivity of the body clusters, we calculated the low-level controlled contrast of [human body (normal - scramble) > monkey body (normal - scramble)] on each body ROI. For each body cluster detected above, the t-values were averaged across all voxels, reflecting the significance of species-selectivity for bodies at a cluster level.

4.7. Group independent component analysis (ICA)

4.7.1. ICA source data

Before performing the group-ICA, physiological and motion confounds were regressed out from the preprocessed functional images. To remove motor-related modulations, the BOLD responses for the catch blocks were removed using the finite impulse response (FIR) model. Twenty-five predictors covering 25 s after the block onset for each catch block were modeled and were then regressed out from the time courses using a GLM. The resulting time courses were then transformed into percentages of signal change to enhance the ICA stability (Allen et al., 2011).

4.7.2. Network extraction

Seventy-five spatial independent components (ICs) were extracted using the Infomax algorithm implemented in the Group ICA of fMRI Toolbox (GIFT, Calhoun et al., 2001). According to previous literature, the model of 75 components is able to cover the known anatomical and functional segmentations (Allen et al., 2011). Individual ICs were back-reconstructed using the GIG-ICA algorithm from the aggregated group ICs (Du and Fan, 2013). The stability of group ICA was assessed by the ICASSO module implemented in the GIFT, which repeated the Infomax decomposition for 20 times and resulted in an index of stability (*Iq*) for each IC (Himberg et al., 2004). To visualize the spatial map of the IC networks, the individual IC maps were normalized to z-scores and averaged across all runs for each participant. A group t-test against zero was computed using the z-scored maps of each subject and corrected using a cluster-threshold statistical procedure based on Monte-Carlo simulation (initial $p < 0.005$, alpha level = 0.05, iteration = 5000).

4.7.3. Body modulation detection

After extraction and back-construction, the individual ICs were analyzed with a data-driven approach. A systematic pipeline was applied to exclude noise components and to find category-modulated networks. ICs with an ICASSO $Iq < 0.8$ were first marked as unstable components and removed (Allen et al., 2011). Next, since the sign of the IC time course was arbitrary, we analyzed the positive and negative parts of each IC separately as different networks with the time courses and spatial maps flipped for the negative ones. We further labeled the white matter (WM) and cerebrospinal fluid (CSF) voxels of each thresholded IC map using customized WM / CSF masks. ICs with more than 10 % WM or CSF voxels were removed as noise signals such as head motions and venous artifacts. Task relevance was modeled for each reconstructed subject-level IC time courses using a GLM with the same design matrix as in the univariate analysis and was conducted for each participant and each run separately. Such a modeling strategy was commonly used to detect the task modulations on IC networks (Beldzik et al., 2013; Jarrahi et al., 2015; Jung et al., 2020). We also assumed a positive HRF response for the cortical network time courses, thus the ICs / flipped ICs with a negative mean beta across all conditions were excluded from further analysis. Finally, we conducted a contrast analysis to find the body-selective networks. The estimated betas were first averaged across all runs for each participant and were then used to calculate the contrast of [normal human body - normal human object] and [human body (normal - scramble) - human object (normal - scramble)]. Right-tailed t-tests and Benjamini-Hochberg multiple comparison corrections were conducted at the group level to find significant body sensitivity.

4.7.4. Condition-omitted ICA

To study the body modulations on node connectivity within networks, we developed a condition-omitted ICA strategy. A human body-omitted dataset was created from the original ICA source data, where in addition to the catch blocks, all normal human body blocks were also regressed out using FIR modeling with 25 predictors per block. A new set of IC was reconstructed from this omitted dataset and the spatial map differences between the original and condition-omitted networks presumably reflect the effect of leaving out human body modulations. Since the estimation of group ICs involves randomization procedures, condition-omitted networks were directly reconstructed from the original aggregated group ICs with GIG-ICA on the new dataset in order to avoid confounds (Du and Fan, 2013).

For the body-selective networks defined above, the difference between the original and condition-omitted maps was computed for each participant and each run. The difference maps were then averaged across runs and entered a group-level t-test against zero and underwent the same cluster-threshold correction. For those human-body-modulated nodes, we expected that their network connectivity would decrease after removing the human body blocks, resulting in lower IC

weights in the condition-omitted maps.

Data Availability

The authors do not have permission to share data.

Acknowledgments

This work was supported by the European Research Council (ERC) FP7-IDEAS-ERC (Grant agreement number 295673; Emobodies), by the ERC Synergy grant (Grant agreement 856495; Relevance), by the Future and Emerging Technologies (FET) Proactive Program H2020-EU.1.2.2 (Grant agreement 824160; EnTimeMent) and by the Industrial Leadership Program H2020-EU.1.2.2 (Grant agreement 825079; MindSpaces).

Competing interests

The authors declare no competing interests.

Appendix A. Supporting information

Supplementary data associated with this article can be found in the online version at doi:10.1016/j.pneurobio.2022.102398.

References

Alcalá-López, D., Smallwood, J., Jefferies, E., Van Overwalle, F., Vogeley, K., Mars, R.B., Turetsky, B.I., Laird, A.R., Fox, P.T., Eickhoff, S.B., Bzdok, D., 2018. Computing the social brain connectome across systems and states. Cereb. Cortex 28, 2207–2232. https://doi.org/10.1093/cercor/bhx121.

Allen, E.A., Erhardt, E.B., Damaraju, E., Gruner, W., Segall, J.M., Silva, R.F., Havlicek, M., Rachakonda, S., Fries, J., Kalyanam, R., Michael, A.M., Caprihan, A., Turner, J.A., Eichele, T., Adelsheim, S., Bryan, A.D., Bustillo, J., Clark, V.P., Ewing, S.W., Filbey, F., Ford, C.C., Hutchison, K., Jung, R.E., Kiehl, K.A., Kodituwakku, P., Komesu, Y.M., Mayer, A.R., Pearlson, G.D., Phillips, J.P., Sadek, J. R., Stevens, M., Teuscher, U., Thoma, R.J., Calhoun, V.D., 2011. A baseline for the multivariate comparison of resting-state networks. Front. Syst. Neurosci. 5, 2. https://doi.org/10.3389/fnsys.2011.00002.

Arcaro, M.J., Pinsk, M.A., Chen, J., Kastner, S., 2018. Organizing principles of pulvino-cortical functional coupling in humans. Nat. Commun. 9, 25–26. https://doi.org/10.1038/s41467-018-077.

Avants, B., Tustison, N.J., Song, G., 2022. Advanced normalization tools: V1.0. Insight J. 2, 1–35. https://doi.org/10.54294/uvnhin.

Beldzik, E., Domagalik, A., Daselaar, S., Fafrowicz, M., Froncisz, W., Oginska, H., Marek, T., 2013. Contributive sources analysis: a measure of neural networks' contribution to brain activations. NeuroImage 76, 304–312. https://doi.org/10.1016/j.neuroimage.2013.03.014.

Borgomaneri, S., Vitale, F., Avenanti, A., 2015. Early changes in corticospinal excitability when seeing fearful body expressions. Sci. Rep. 5, 1–9. https://doi.org/10.1038/srep14122.

Breman, H., Mulders, J., Fritz, L., Peters, J., Pyles, J., Eck, J., Bastiani, M., Roebroeck, A., Ashburner, J., Goebel, R., 2020. An image registration-based method for epi distortion correction based on opposite phase encoding (cope). Lecture notes in computer science (including subseries lecture notes in artificial intelligence and lecture notes in bioinformatics) 12120. LNCS 122–130. https://doi.org/10.1007/978-3-030-50120-4_12.

Briggs, R.G., Chakraborty, A.R., Anderson, C.D., Abraham, C.J., Palejwala, A.H., Conner, A.K., Pelargos, P.E., O'Donoghue, D.L., Glenn, C.A., Sughrue, M.E., 2019. Anatomy and white matter connections of the inferior frontal gyrus. Clin. Anat. 32, 546–556. https://doi.org/10.1002/ca.23349.

Calhoun, V., Adali, T., Pearlson, G., Pekar, J., 2001. A method for making group inferences from functional mri data using independent component analysis. Hum. Brain Mapp. 14, 140–151. https://doi.org/10.1002/hbm.1048.

Candidi, M., Stienen, B.M., Aglioti, S.M., de Gelder, B., 2015. Virtual lesion of right posterior superior temporal sulcus modulates conscious visual perception of fearful expressions in faces and bodies. Cortex 65, 184–194. https://doi.org/10.1016/j.cortex.2015.01.012.

Caspers, S., Zilles, K., Laird, A.R., Eickhoff, S.B., 2010. Ale meta-analysis of action observation and imitation in the human brain. NeuroImage 50, 1148–1167. https://doi.org/10.1016/j.neuroimage.2009.12.112.

Cheng, L., Zhang, Y., Li, G., Wang, J., Sherwood, C., Gong, G., Fan, L., Jiang, T., 2021. Connectional asymmetry of the inferior parietal lobule shapes hemispheric specialization in humans, chimpanzees, and rhesus macaques. eLife 10, e67600. https://doi.org/10.7554/eLife.67600.

Collins, D.L., Neelin, P., Peters, T.M., Evans, A.C., 1994. Automatic 3d intersubject registration of MR volumetric data in standardized talairach space. J. Comput. Assist. Tomogr. 18, 192–205. https://doi.org/10.1097/00004728-199403000-00005.

Corbetta, M., Patel, G., Shulman, G.L., 2008. The reorienting system of the human brain: From environment to theory of mind. Neuron 58, 306–324. https://doi.org/10.1016/j.neuron.2008.04.017.

De Winter, F.L., Zhu, Q., Van den Stock, J., Nelissen, K., Peeters, R., de Gelder, B., Vanduffel, W., Vandenbulcke, M., 2015. Lateralization for dynamic facial expressions in human superior temporal sulcus. NeuroImage 106, 340–352. https://doi.org/10.1016/j.neuroimage.2014.11.020.

Downing, P., Kanwisher, N., 2001. A cortical area specialized for visual processing of the human body. J. Vis. 1, 2470–2473. https://doi.org/10.1167/1.3.341.

Du, Y., Fan, Y., 2013. Group information guided ica for fmri data analysis. NeuroImage 69, 157–197. https://doi.org/10.1016/j.neuroimage.2012.11.008.

Du, Y., Pearlson, G.D., Lin, D., Sui, J., Chen, J., Salman, M., Tamminga, C.A., Ivleva, E.I., Sweeney, J.A., Keshavan, M.S., Clementz, B.A., Bustillo, J., Calhoun, V.D., 2017. Identifying dynamic functional connectivity biomarkers using gig-ica: application to schizophrenia, schizoaffective disorder, and psychotic bipolar disorder. Hum. Brain Mapp. 38, 2683–2708. https://doi.org/10.1002/hbm.23553.

Errante, A., Rossi Sebastiano, A., Ziccarelli, S., Bruno, V., Rozzi, S., Pia, L., Fogassi, L., Garbarini, F., 2022. Structural connectivity associated with the sense of body ownership: a diffusion tensor imaging and disconnection study in patients with bodily awareness disorder. Brain Commun. 4, fcac032. https://doi.org/10.1093/braincomms/fcac032.

de Gelder, B., Poyo Solanas, M., 2021. A computational neuroethology perspective on body and expression perception. Trends Cogn. Sci. 25, 744–756. https://doi.org/10.1016/j.tics.2021.05.010.

de Gelder, B., Snyder, J., Greve, D., Gerard, G., Hadjikhani, N., 2004. Fear fosters flight: a mechanism for fear contagion when perceiving emotion expressed by a whole body. Proc. Natl. Acad. Sci. USA 101, 16701–16706. https://doi.org/10.1073/pnas.0407042101.

de Gelder, B., den Stock, Van, Meeren, J., Sinke, H.K., Kret, C.B., Tamietto, M, M.E., 2010. Standing up for the body. recent progress in uncovering the networks involved in the perception of bodies and bodily expressions. Neurosci. Biobehav. Rev. 34, 513–527. https://doi.org/10.1016/j.neubiorev.2009.10.008.

Geng, J.J., Vossel, S., 2013. Re-evaluating the role of TPJ in attentional control: contextual updating. Neurosci. Biobehav. Rev. 37, 2608–2620. https://doi.org/10.1016/j.neubiorev.2013.08.010.

Glover, G.H., Li, T., Ress, D., 2000. Image-based method for retrospective correction of physiological motion effects in fmri: retroicor. Magn. Reson. Med. 44, 162–167. https://doi.org/10.1002/1522-2594(200007)44:13.3.CO;2-5.

Goebel, R., 2012. Brainvoyager — past, present, future. NeuroImage 62, 748–756. https://doi.org/10.1016/j.neuroimage.2012.01.083.

Goldberg, H., Preminger, S., Malach, R., 2014. The emotion-action link? naturalistic emotional stimuli preferentially activate the human dorsal visual stream. NeuroImage 84, 254–264. https://doi.org/10.1016/j.neuroimage.2013.08.032.

Grabenhorst, F., Rolls, E.T., 2011. Value, pleasure and choice in the ventral prefrontal cortex. Trends Cogn. Sci. 15, 56–67. https://doi.org/10.1016/j.tics.2010.12.004.

Greve, D.N., Fischl, B., 2009. Accurate and robust brain image alignment using boundary-based registration. NeuroImage 48, 63–72. https://doi.org/10.1016/j.neuroimage.2009.06.060.

Grèzes, J., Pichon, S., de Gelder, B., 2007. Perceiving fear in dynamic body expressions. NeuroImage 35, 959–967. https://doi.org/10.1016/j.neuroimage.2006.11.030.

Grill-Spector, K., Sayres, R., 2008. Object recognition: Insights from advances in fmri methods. Curr. Dir. Psychol. Sci. 17, 73–79. https://doi.org/10.1111/j.1467-8721.2008.00552.x.

Grill-Spector, K., Weiner, K.S., 2014. The functional architecture of the ventral temporal cortex and its role in categorization. Nat. Rev. Neurosci. 15, 536–548. https://doi.org/10.1038/nrn3747.

Gross, C.G., Bender, D.B., Rocha-Miranda, C.E., 1969. Visual receptive fields of neurons in inferotemporal cortex of the monkey. Science 166, 1303–1306. https://doi.org/10.1126/science.166.3910.1303.

Haak, K.V., Beckmann, C.F., 2018. Objective analysis of the topological organization of the human cortical visual connectome suggests three visual pathways. Cortex 98, 73–83. https://doi.org/10.1016/j.cortex.2017.03.020.

Hadjikhani, N., De Gelder, B., 2003. Seeing fearful body expressions activates the fusiform cortex and amygdala. Curr. Biol. 13, 2201–2205. https://doi.org/10.1016/j.cub.2003.11.049.

Hartwigsen, G., Neef, N.E., Camilleri, J.A., Margulies, D.S., Eickhoff, S.B., 2019. Functional segregation of the right inferior frontal gyrus: evidence from coactivation-based parcellation. Cereb. Cortex 29, 1532–1546. https://doi.org/10.1093/cercor/bhy049.

Harvey, A.K., Pattinson, K.T., Brooks, J.C., Mayhew, S.D., Jenkinson, M., Wise, R.G., 2008. Brainstem functional magnetic resonance imaging: Disentangling signal from physiological noise. J. Magn. Reson. Imaging 28, 1337–1344. https://doi.org/10.1002/jmri.21623.

Hasson, U., Yang, E., Vallines, I., Heeger, D.J., Rubin, N., 2008. A hierarchy of temporal receptive windows in human cortex. J. Neurosci. 28, 2539–2550. https://doi.org/10.1523/JNEUROSCI.5487-07.2008.

Hasson, U., Chen, J., Honey, C.J., 2015. Hierarchical process memory: memory as an integral component of information processing. Trends Cogn. Sci. 19, 304–313. https://doi.org/10.1016/j.tics.2015.04.006.

Himberg, J., Hyvärinen, A., Esposito, F., 2004. Validating the independent components of neuroimaging time series via clustering and visualization. NeuroImage 22, 1214–1222. https://doi.org/10.1016/j.neuroimage.2004.03.027.

Hortensius, R., Terburg, D., Morgan, B., Stein, D.J., van Honk, J., de Gelder, B., 2017. The dynamic consequences of amygdala damage on threat processing in urbach–wiethe disease. a commentary on pishnamazi et al. (2016). Cortex 88, 192–197. https://doi.org/10.1016/j.cortex.2016.07.013.

Igelström, K.M., Graziano, M.S., 2017. The inferior parietal lobule and temporoparietal junction: a network perspective. Neuropsychologia 105, 70–83. https://doi.org/10.1016/j.neuropsychologia.2017.01.001.

Jarrahi, B., Mantini, D., Balsters, J.H., Michels, L., Kessler, T.M., Mehnert, U., Kollias, S. S., 2015. Differential functional brain network connectivity during visceral interoception as revealed by independent component analysis of fmri time-series. Hum. Brain Mapp. 36, 4438–4468. https://doi.org/10.1002/hbm.22929.

Jung, J.Y., Bungert, A., Bowtell, R., Jackson, S.R., 2020. Modulating brain networks with transcranial magnetic stimulation over the primary motor cortex: a concurrent tms/fmri study. Front. Hum. Neurosci. 14, 31. https://doi.org/10.3389/fnhum.2020.00031.

Koster-Hale, J., Saxe, R., 2013. Theory of mind: a neural prediction problem. Neuron 79, 836–848. https://doi.org/10.1016/j.neuron.2013.08.020.

Kret, M.E., Pichon, S., Grèzes, J., De Gelder, B., 2011. Similarities and differences in perceiving threat from dynamic faces and bodies. an fmri study. NeuroImage 54, 1755–1762. https://doi.org/10.1016/j.neuroimage.2010.08.012.

Long, B., Yu, C.P., Konkle, T., 2018. Mid-level visual features underlie the high-level categorical organization of the ventral stream. Proc. Natl. Acad. Sci. USA 115, E9015–E9024. https://doi.org/10.1073/pnas.1719616115.

Mars, R.B., Sallet, J., Schüffelgen, U., Jbabdi, S., Toni, I., Rushworth, M.F.S., 2011. Connectivity-based subdivisions of the human right "temporoparietal junction area": evidence for different areas participating in different cortical networks. Cereb. Cortex 22, 1894–1903. https://doi.org/10.1093/cercor/bhr268.

Nachev, P., Kennard, C., Husain, M., 2008. Functional role of the supplementary and presupplementary motor areas. Nat. Rev. Neurosci. 9, 856–869. https://doi.org/10.1038/nrn2478.

Orban, G., Lanzilotto, M., Bonini, L., 2021. From observed action identity to social affordances. Trends Cogn. Sci. 25, 493–505. https://doi.org/10.1016/j.tics.2021.02.012.

Padmala, S., Lim, S.L., Pessoa, L., 2010. Pulvinar and affective significance: responses track moment-to-moment stimulus visibility. Front. Hum. Neurosci. 4. https://doi.org/10.3389/fnhum.2010.00064.

Panksepp, J., 1989. The neurobiology of emotions: of animal brains and human feelings. Handbook of social psychophysiology. Wiley Handb. Psychophysiol. 5–26.

Patel, G.H., Sestieri, C., Corbetta, M., 2019. The evolution of the temporoparietal junction and posterior superior temporal sulcus. Cortex 118, 38–50. https://doi.org/10.1016/j.cortex.2019.01.026.

Patel, G.H., Arkin, S.C., Ruiz-Betancourt, D.R., Plaza, F.I., Mirza, S.A., Vieira, D.J., Strauss, N.E., Klim, C.C., Sanchez-Peña, J.P., Bartel, L.P., et al., 2021. Failure to engage the temporoparietal junction/posterior superior temporal sulcus predicts impaired naturalistic social cognition in schizophrenia. Brain 144, 1898–1910. https://doi.org/10.1093/brain/awab081.

Peelen, M.V., Downing, P.E., 2005. Selectivity for the human body in the fusiform gyrus. J. Neurophysiol. 93, 603–608. https://doi.org/10.1152/jn.00513.2004.

Peelen, M.V., Atkinson, A.P., Andersson, F., Vuilleumier, P., 2007. Emotional modulation of body-selective visual areas. Soc. Cogn. Affect. Neurosci. 2, 274–283. https://doi.org/10.1093/scan/nsm023.

Pessoa, L., Adolphs, R., 2010. Emotion processing and the amygdala: from a 'low road' to 'many roads' of evaluating biological significance. Nat. Rev. Neurosci. 11, 773–782. https://doi.org/10.1038/nrn2920.

Pessoa, L., Japee, S., Sturman, D., Ungerleider, L.G., 2006. Target visibility and visual awareness modulate amygdala responses to fearful faces. Cereb. Cortex 16, 366–375. https://doi.org/10.1093/cercor/bhi115.

Pichon, S., de Gelder, B., Grèzes, J., 2009. Two different faces of threat. comparing the neural systems for recognizing fear and anger in dynamic body expressions. NeuroImage 47, 1873–1883. https://doi.org/10.1016/j.neuroimage.2009.03.084.

Pichon, S., De Gelder, B., Grèzes, J., 2012. Threat prompts defensive brain responses independently of attentional control. Cereb. Cortex 22, 274–285. https://doi.org/10.1093/cercor/bhr060.

Pitcher, D., Ungerleider, L.G., 2021. Evidence for a third visual pathway specialized for social perception. Trends Cogn. Sci. 25, 100–110. https://doi.org/10.1016/j.tics.2020.11.006.

Polosecki, P., Moeller, S., Schweers, N., Romanski, L.M., Tsao, D.Y., Freiwald, W.A., 2013. Faces in motion: selectivity of macaque and human face processing areas for dynamic stimuli. J. Neurosci. 33, 11768–11773. https://doi.org/10.1523/JNEUROSCI.5402-11.2013.

Poyo Solanas, M., Vaessen, M., De Gelder, B., 2020a. Computation-based feature representation of body expressions in the human brain. Cereb. Cortex 30, 6376–6390. https://doi.org/10.1093/cercor/bhaa196.

Poyo Solanas, M., Vaessen, M.J., de Gelder, B., 2020b. The role of computational and subjective features in emotional body expressions. Sci. Rep. 10, 1–13. https://doi.org/10.1038/s41598-020-63125-1.

Ptak, R., Schnider, A., Fellrath, J., 2017. The dorsal frontoparietal network: a core system for emulated action. Trends Cogn. Sci. 21, 589–599. https://doi.org/10.1016/j.tics.2017.05.002.

Ross, P., de Gelder, B., Crabbe, F., Grosbras, M.H., 2020. A dynamic body-selective area localizer for use in fmri. MethodsX 7. https://doi.org/10.1016/j.mex.2020.100801.

Sato, W., Kochiyama, T., Uono, S., Sawada, R., Kubota, Y., Yoshimura, S., Toichi, M., 2019. Widespread and lateralized social brain activity for processing dynamic facial expressions. Hum. Brain Mapp. 40, 3753–3768. https://doi.org/10.1002/hbm.24629.

Saxe, R., Kanwisher, N., 2003. People thinking about thinking people: the role of the temporoparietal junction in "theory of mind". NeuroImage 19, 1835–1842. https://doi.org/10.1016/S1053-8119(03)00230-1.

Scheliga, S., Schwank, R., Scholle, R., Habel, U., Kellermann, T., 2022. A neural mechanism underlying predictive visual motion processing in patients with schizophrenia. Psychiatry Res. 318, 114934 https://doi.org/10.1016/j.psychres.2022.114934.

Schurz, M., Radua, J., Aichhorn, M., Richlan, F., Perner, J., 2014. Fractionating theory of mind: a meta-analysis of functional brain imaging studies. Neurosci. Biobehav. Rev. 42, 9–34. https://doi.org/10.1016/j.neubiorev.2014.01.009.

Schwarzlose, R.F., Baker, C.I., Kanwisher, N., 2005. Separate face and body selectivity on the fusiform gyrus. J. Neurosci. 25, 11055–11059. https://doi.org/10.1523/JNEUROSCI.2621-05.2005.

Taubert, J., Ritchie, J.B., Ungerleider, L.G., Baker, C.I., 2022. One object, two networks? assessing the relationship between the face and body-selective regions in the primate visual system. Brain Struct. Funct. 227, 1423–1438. https://doi.org/10.1007/s00429-021-02420-7.

Utter, A.A., Basso, M.A., 2008. The basal ganglia: an overview of circuits and function. Neurosci. Biobehav. Rev. 32, 333–342. https://doi.org/10.1016/j.neubiorev.2006.11.003.

Van Overwalle, F., 2009. Social cognition and the brain: a meta-analysis. Hum. Brain Mapp. 30, 829–858. https://doi.org/10.1002/hbm.20547.

Vogels, R., 2022. More than the face: representations of bodies in the inferior temporal cortex. Annu. Rev. Vis. Sci. 8. https://doi.org/10.1146/annurev-vision-100720-113429.

Vossel, S., Geng, J.J., Fink, G.R., 2014. Dorsal and ventral attention systems: distinct neural circuits but collaborative roles. Neuroscientist 20, 150–159. https://doi.org/10.1177/1073858413494269.

Weiner, K.S., Grill-Spector, K., 2011. Not one extrastriate body area: using anatomical landmarks, hmt+, and visual field maps to parcellate limb-selective activations in human lateral occipitotemporal cortex. NeuroImage 56, 2183–2199. https://doi.org/10.1016/j.neuroimage.2011.03.041.

Yokoyama, C., Autio, J.A., Ikeda, T., Sallet, J., Mars, R.B., Van Essen, D.C., Glasser, M.F., Sadato, N., Hayashi, T., 2021. Comparative connectomics of the primate social brain. NeuroImage 245. https://doi.org/10.1016/j.neuroimage.2021.118693.

Young, L., Dodell-Feder, D., Saxe, R., 2010. What gets the attention of the temporo-parietal junction? an fmri investigation of attention and theory of mind. Neuropsychologia 48, 2658–2664. https://doi.org/10.1016/j.neuropsychologia.2010.05.012.

Yovel, G., O'Toole, A.J., 2016. Recognizing people in motion. Trends Cogn. Sci. 20, 383–395. https://doi.org/10.1016/j.tics.2016.02.005.

Zhu, Q., Nelissen, K., Van den Stock, J., De Winter, F.L., Pauwels, K., de Gelder, B., Vanduffel, W., Vandenbulcke, M., 2013. Dissimilar processing of emotional facial expressions in human and monkey temporal cortex. Neuroimage 66, 402–411. https://doi.org/10.1016/j.neuroimage.2012.10.083.